PASJ: Publ. Astron. Soc. Japan **48**, 511–528 (1996)

Line-Profile Analysis of K I 7699 in the Sun and in Procyon

Yoichi TAKEDA
Institute of Astronomy, The University of Tokyo, Mitaka, Tokyo 181
E-mail: takedayi@cc.nao.ac.jp

Ken-ichi KATO and Yoshiya WATANABE
Science Museum of Osaka, Nakanoshima, Kita-ku, Osaka 530
and
Kozo SADAKANE
Astronomical Institute, Osaka Kyoiku University, Asahigaoka, Kashiwara, Osaka 582

(Received 1995 July 21; accepted 1996 February 23)

Abstract

The profiles of the resonance line of potassium (K I 7698.98) in the flux spectrum of the Sun and Procyon were studied in detail using the multi-parameter fitting method, in order to extract information regarding the fundamental atomic parameters responsible for the formation of this line as well as to diagnose the nature of the velocity fields in their atmospheres. It was concluded from an analysis of the solar K I 7699 profile that neutral-hydrogen collisions are practically negligible compared to electron collisions in the rate equation of statistical equilibrium, and that an empirical correction to the Unsöld's standard (van der Waals effect) damping constant is $\Delta \log C_6 \simeq +1.0$ with the most consistent microturbulent velocity of $\xi \simeq 0.8$ km s^{-1}. Based upon these results, the atmospheric-velocity parameters of Procyon were determined to be $\xi \simeq 1.4$ km s^{-1}, $\zeta_{\rm RT} \simeq 6.7$ km s^{-1} (the radial-tangential macroturbulence), and $v_{\rm e} \sin i \simeq 3.3$ km s^{-1} (the projected rotational velocity). The potassium abundances of the Sun and Procyon derived from this resonance line, which are significantly affected by the non-LTE effect amounting to ~ 0.4 dex (Sun) and ~ 0.7 dex (Procyon), turned out to be nearly the same and $\log \epsilon_{\rm K} \simeq 5.1$. It also appears that the microturbulence tends to decrease with an increase in the atmospheric height of the Sun as well as of Procyon.

Key words: Line formation — Line profiles — Stars: abundances — Stars: individual (Procyon) — Sun: atmosphere

1. Introduction

The role played by the resonance line of potassium is known to be significant in the spectroscopy of solar-type stars. Although the stronger line at 7664.87 Å is usually not usable, because of being badly contaminated by a telluric O_2 line, the profile of the counterpart line at 7698.98 Å has been widely used for the purpose of diagnosing the physical condition of the surface layer of a star, especially in the field of solar/stellar seismology or hydrodynamics. That is, its saturated large strength with a fairly clean profile practically free from any blending, coupled with large sensitivity to any variation in T (temperature) or P (pressure), because of the low ionization potential (4.34 eV) of neutral potassium, makes this line quite suitable for investigating dynamical phenomena in stellar atmospheres (such as stellar granulation, wave propagation, and oscillation) by detecting subtle asymmetries or temporal changes in its profile.

Unfortunately, however, we do not yet have a clear understanding regarding the formation of this line. For example, this strong resonance line is known to suffer an appreciable non-LTE effect. Though this point has so far been elaborately studied by several investigators (see Bruls et al. 1992 and the references therein), there remains a very important problem of how to treat collisions with H I (neutral hydrogen) atoms in the rate equation of kinetic equilibrium (cf. Lambert 1993 for a review), which seems to still be unexplored and unsettled, at least for potassium. Also, since this line has a fairly large strength in solar-type stars, its profile is appreciably affected by the (van der Waals) damping constant, which is yet to be firmly established because of being presently subject to considerable uncertainties. It is therefore worthwhile and desirable to obtain empirical information regarding these points by way of closely investigating the line profile of K I 7699 in the spectrum of the Sun, the most extensively studied star so far, for which observational data of very high quality as well as sufficiently reliable atmospheric models are available.

Recently, an efficient technique for studying stellar line profiles has been developed by Takeda (1995a; hereinafter referred to as Paper I), which we call "the multi-parameter fitting method" (hence abbreviated as the MPF method). As a matter of fact, this method has proved to be quite effective for investigating atmospheric velocity fields (e.g., separating rotation from turbulence) in β Ori (Takeda et al. 1995; Paper II) and in the Sun (Takeda 1995b; Paper III). Furthermore, Takeda (1995c; Paper IV) has shown, in his analyses of the lines of oxygen (O I 7771–5) and sodium (Na I 8183/95) in the solar flux spectrum, that this MPF technique can be successfully applied to the very purpose mentioned above: i.e., to determining the empirical corrections to the widely used standard classical formulae for the H I collision rates or van der Waals damping constants.

Hence, this paper is regarded as being the fifth of the series. Namely, we aim in this study, extending and closely following the analysis of Paper IV, to extract information regarding such atomic parameters of potassium from the profile of K I 7699 in the solar flux spectrum, while establishing the potassium abundance of the Sun by correctly taking into account the non-LTE effect. This was the primary purpose of the present investigation.

Then, equipped with these results of atomic parameters, we applied our MPF method to the K I 7699 profile of Procyon (α CMi), the well-known bright F5 IV–V star which is often referred to as an important standard for studying solar-type stars, in order to settle the photospheric abundance of K as well as to study the velocity fields in its atmosphere; more precisely, to determine $v_{\rm e}\sin i$ (rotational velocity), $\zeta_{\rm RT}$ (radial-tangential macroturbulence), and ξ (microturbulence) separately from each other, such as was done in Papers II and III. This would be another interesting challenge and touchstone for our MPF technique, since this difficult task has so-far been tried only by using the Fourier-transform method (e.g., Wynne-Jones et al. 1978; Gray 1981; de Jager, Neven 1982). That makes the second topic of this study.

We realized in the course of Procyon's study that it is essential to establish the most reasonable model parameters for this star in order to accomplish an accurate abundance-determination. We therefore decided to re-determine $T_{\rm eff}$ (effective temperature) and $\log g$ (surface gravity) by ourselves based on its energy distribution, while taking into consideration how the convection mixing length (l/H; expressed in unit of the pressure scale height H) affects the results. In this connection, we also reanalyzed the published equivalent-width data of iron-group elements with the updated recent gf values, in order to establish the scale of microturbulence as well as to examine the consistency of the resulting abundances between neutral and ionized species (i.e., the condition of ionization balance). These supplementary analyses with respect to Procyon are described in appendices 1, 2, and 3.

2. Model Atmospheres

In order to maintain consistency with our previous studies (e.g., Takeda 1994a, or Paper IV), our standard atmospheric models for the Sun and Procyon adopted in this study basically stem from the ATLAS6 models published by Kurucz (1979), the parameters ($T_{\rm eff}$, $\log g$, l/H) of which are (5770, 4.44, 2.0) and (6500, 4.0, 2.0), respectively. As was done in Paper IV, we test in this section two kinds of solar models which were constructed by extending the original one; the Model-E is a simply extrapolated model (from $\tau_{5000} = 10^{-6}$ to 10^{2}) with systematically decreasing temperature outwards, whereas Model-C has a chromospheric $T(\tau_{5000})$ distribution of Maltby et al.'s (1985) reference solar model at $\tau_{5000} \leq 10^{-3}$ (while the temperature structure at $10^{-3} \leq \tau_{5000}$ is the same as that of Model-E). Regarding Procyon, we used throughout this study an extrapolated model (hereinafter called Model-P), which was prepared in a similar manner to the case of Model-E for the Sun.

3. Non-LTE Calculations

3.1. *Procedures*

Our statistical equilibrium calculations on neutral potassium were conducted similarly to the case of sodium (cf. Takeda, Takada-Hidai 1994). We included all of the K I energy levels listed in Moore (1971), and all radiatively permitted K I transitions compiled in Kurucz and Peytremann (1975) with the transition probabilities given therein. In addition, we also consulted Wiese et al. (1969) for 4 transition arrays missing in their compilation. Combining the levels/transitions belonging to a common (LS) term/multiplet into a single term/transition as usual, we eventually obtained an atomic model comprising 106 K I terms up to the principal quantum number $n = 79$ (plus one ground term of K II) and 269 radiative transitions connecting these terms.

Regarding the photoionization cross section (α_ν), the detailed ν-dependence was taken into account only for the ground term ($4s\,^2S$) and the first excited term ($4p\,^2P^o$), according to Mathisen (1984) and Aymar et al. (1976), respectively; otherwise, we adopted the edge-values presented in table 1 of Bruls et al. (1992) for the 17 excited terms up to $6g\,^2G$ and those calculated by the hydrogenic approximation (Travis, Matsushima 1968) for all of the remaining terms, assuming $\alpha_\nu \propto \nu^{-3}$.

As was done in Paper IV, we introduced a free parameter (h) for controlling the contribution of neutral-

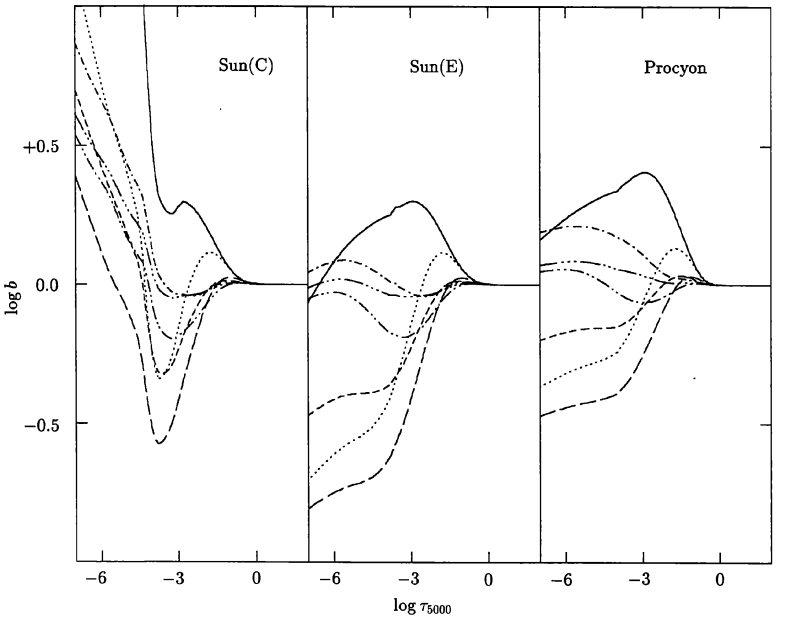

Fig. 1. Run of the non-LTE departure coefficients (b_α) of the representative seven K I terms with the standard continuum optical depth at 5000Å (τ_{5000}). [Note that what was remarked in the caption of Takeda and Takada-Hidai's (1995) figure 1 also holds for this case.] The results displayed here are those computed with $h = -3$ on our standard reference models for the Sun and Procyon; Model-C (left), Model-E (middle), and Model-P (right). See section 2 for the details of the calculations. The solid line, dotted line, short-dashed line, long-dashed line, dash-dotted line, dash-double-dotted line, and the dash-triple-dotted line correspond to the terms $4s\,^2S$, $4p\,^2P^o$, $5s\,^2S$, $3d\,^2D$, $5p\,^2P^o$, $4d\,^2D$, and $6s\,^2S$, respectively.

hydrogen collisions. Namely, the collisional rates appearing in the equations of statistical equilibrium are expressed as $C_e(1C) + 10^h C_H(1C)$, where $C_e(1C)$ and $C_H(1C)$ (each corresponding to electron- and H I-collision rates) are such those evaluated following the standard recipe which was called "1C Case" and was decribed in detail by Takeda (1994a); various values ranging from -3.0 to $+0.5$ were assigned to this parameter, in order to see how the results are affected by its change.

3.2. *Computational Results*

The resulting b-values (the departure coefficients) of the lower representative terms for the case $h = -3$ (i.e., the finally adopted case corresponding to practically neglecting H I collisions; see section 4), which were calculated with the solar potassium abundance and a depth-independent microturbulence of 1 km s^{-1} (Sun) or 2 km s^{-1} (Procyon) on the already described standard model atmospheres, are displayed in figure 1.

The effects of changing h on the line opacity and the line source function for the resonance transition corresponding to K I 7699 are shown in figure 2; there, we see that the results for $h \lesssim -2$ are no more sensitive to h and hardly dicernible from each other, which means that C_H becomes practically of negligible importance compared to C_e already at $h \simeq -2$ [recall the relation $C_H(1C)/C_e(1C) \lesssim 10^2$ at $\tau_{5000} \sim 10^{-1}$; see subsection 5.1 in Paper IV].

The influences of h on the line profile of K I 7699 are depicted in figure 3, where we can clearly recognize that the deepening of the core (i.e., a characteristic non-LTE effect) is progressively enhanced along with a decrease in h. Note that the Model-E results for the Sun are not shown any more in this figure because of being essentially the same as those of Model-C shown here, reflecting that the non-LTE K I populations are inert to any change in the local electron-temperature (T_e) because of their fairly weak T_e-dependence ($\propto T_e^{-1/2}$) for such an alkali element being mostly ionized (cf. subsection 2.4 in Paper IV). For this reason, we will exclusively use Model-C for the analysis of the solar K I 7699 profile (see subsection 4.3).

Generally speaking, the results for the Sun presented in our figures 1–3 are satisfactorily compared with those in figures 6 and 7 of Bruls et al. (1992); this indicates the consistency of both independent calculations.

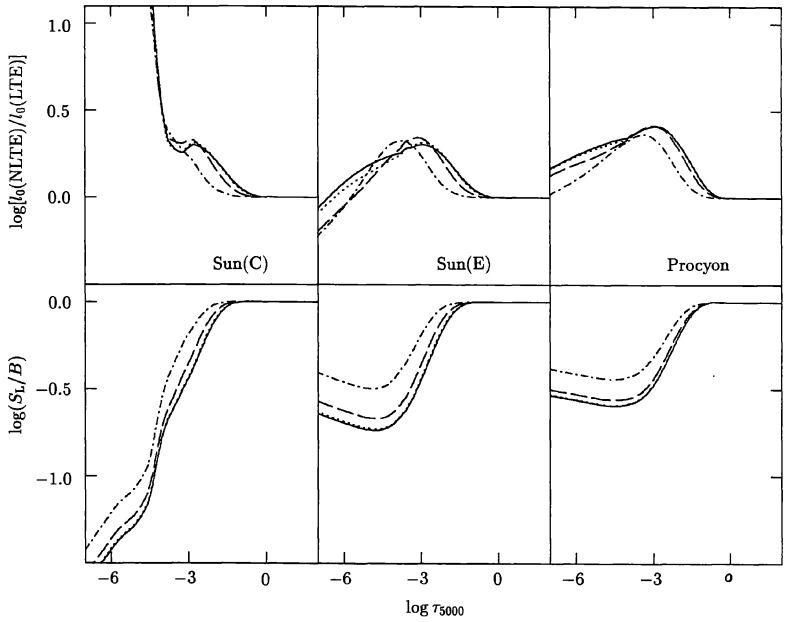

Fig. 2. Depth-dependence of the non-LTE to LTE opacity ratio (upper panels) as well as of the line source function (S_L) in unit of the local Planck function (B) (lower panels) for the resonance transition ($4s\,^2S$–$4p\,^2P^o$) corresponding to K I 7699. Those displayed are the results calculated for the same model atmospheres as in figure 1 with three different h values; $h = -3$ (solid line), -2 (dotted line), -1 (dashed line), and 0 (dash-dotted line).

4. Profile Analysis

4.1. Observational Data

Regarding the observational profile data of K I 7699 for the Sun, we invoked, as in Paper IV, the disk-integrated solar flux spectrum published by Kurucz et al. (1984), which was obtained by them with the Fourier-transform spectrometer on the McMath Solar Telescope at Kitt Peak National Observatory, and has a very high spectral resolving power ($R = 523000$ for this wavelength region) as well as a very high signal-to-noise ratio (several thousands).

Meanwhile, the line profile of K I 7699 for Procyon is based on our own data, which was observed on 1994 February 1.7 (UT) by using the CCD-equipped coude spectrograph attached to the 65cm solar telescope at Okayama Astrophysical Observatory. See Kato et al. (1995) for more details concerning the observations and the data reduction. The K I 7699 profile of Procyon adopted for our analysis is shown in figure 4, where it has been normalized with respect to the empirically estimated continuum, similarly to Kurucz et al.'s (1984) data for the Sun (though such a normalization is actually not necessary for our MPF method). This spectrum has a S/N ratio of $\sim$ 150, while the spectral resolution was estimated to be $\sim$ 150000 from the typical FWHM width (~ 2 km s^{-1}) of the comparison lines. Note that we applied appropriate corrections by hand to the slight distortions found in the redward wing and the core of the profile. We believe that this feature is attributed to an unfavorable instrumental effect, since removal of CCD interferance fringes at the Okayama solar coude spectrograph turned out to be occasionally unsatisfactory, depending on wavelength regions, which then leaves a slight wavy (or ripple-like) pattern in the reduced spectrum (see Kato et al. 1995).

4.2. Method and Computational Details

In the present application of our MPF method (see Paper I for its basic concept) to the profile of K I 7699, the parameters of our interest are mostly the same as those in Paper IV (though some of these are fixed depending on cases): the potassium abundance ($\log \epsilon_K$), the microturbulence (ξ), the radial-tangential macroturbulence (ζ_{RT}), the projected rotational velocity ($v_e \sin i$), the wavelength shift ($\Delta\lambda_r$), the H I-collision parameter (h), and the van der Waals damping correction ($\Delta \log C_6$) applied to Unsöld's (1955) classical formula. Hence, the theoretical synthetic fluxes (F_{λ_i}) at each of the wavelength points are computable when these seven param-

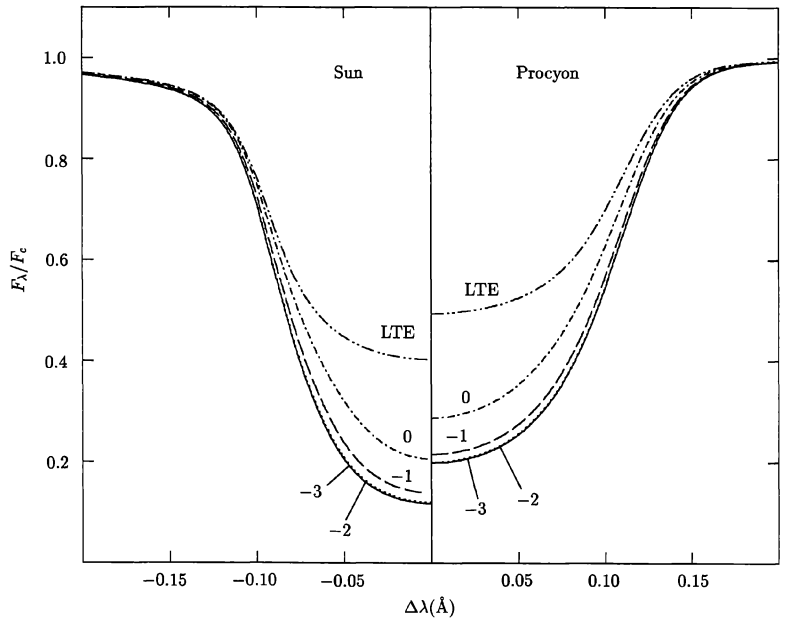

Fig. 3. Theoretical non-LTE flux profiles of K I 7699 (without being macro-broadened) computed with $\log \epsilon_K = 5.12$ (the solar potassium abundance adopted from Anders and Grevesse 1984) and three different h values for the Sun (Model-C with ξ= 1km s^{-1}; left-hand panel) and Procyon (Model-P with ξ= 2km s^{-1}; right-hand panel), which are displayed with the same meanings of the line-types as in figure 2. The corresponding LTE profiles ($h = +\infty$) are also shown by dash-double-dotted lines for a comparison.

eters are given, following the same way as described in subsection 3.3 of Paper IV. As for the instrumental profile, we adopted a "sinc" function corresponding to a resolving power of $R = 523000$ for the Sun (cf. section 4 of Paper III) and a Gaussian function with FWHM = 2 km s^{-1} for Procyon. Regarding the atomic parameters of K I 7699 other than the van der Waals effect damping constant (to be controlled with $\Delta \log C_6$), we adopted $\log gf = -0.169$ (Wiese et al. 1969) for the oscillator strength, $\Gamma_{\rm rad} = 0.382 \times 10^8$ s^{-1} (Wiese et al. 1969) for the radiation damping constant, and the formulae of Griem (1974) (with the data given therein) for the quadratic Stark effect damping width.

4.3. Remark on the Meaning of ξ

Before describing the detailed procedures and results of our analysis, it is necessary to clarify the meaning of the microturbulence considered in the present study. As is well known, this quantity is nothing but a useful fudge parameter, which is introduced (as a depth-independent thermal-motion-like microscopic velocity-dispersion) so as to fulfill the postulated requirements (see below) when one wishes to extract any information from the spectral features of saturated lines. It should be here pointed out that there are two kinds of microturbulence reflecting the difference of consistency that we demand:

(i) For one thing, we may require that one should obtain the correct abundance of the concerned element (e.g., settled by other weak lines) by an appropriate choice of ξ. In other words, this is the conventional "curve-of-growth-type" microturbulence familiar to us, which we explicitly designate as $\xi_{\rm A}$ (abundance-constrained ξ).

(ii) The other alternative is that ξ be so chosen as to accomplish the best-fit of the profile among all possible cases *regardless of the resulting abundance.* We refer to the microturbulence of this meaning as $\xi_{\rm P}$ (profile-fit ξ).

These two types of ξ should yield the same value, if such a simple depth-independent Gaussian-microturbulence modeling is strictly realistic. Unfortunately, however, we can not expect such an ideal situation to actually hold. Thus, these two ξ values would naturally turn out to be more or less discrepant from each other, reflecting the modeling-incompleteness. As a matter of fact, this kind of discordance has occasionally been reported from several profile analyses [e.g., Smith (1973) for A stars, or Paper III for the Sun]. Nevertheless, this parameter may still remain useful even in such circumstances, if one is alert to its applicability-limit without confusing these two different meanings.

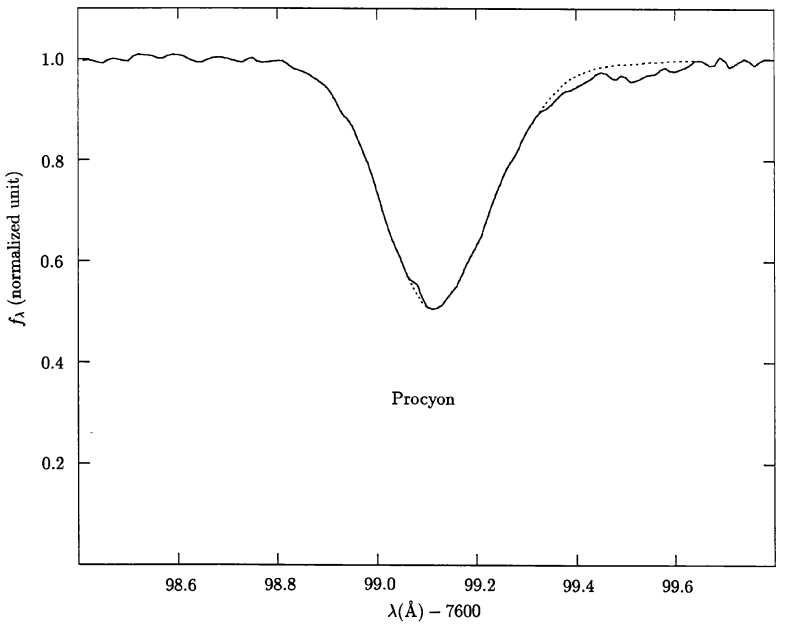

Fig. 4. Observed K I 7699 profile of Procyon used for our analysis, being normalized with respect to the empirically determined continuum level. The original raw profile is indicated by the solid line, while the dotted line indicates the corrected profile for those presumable defects seen at the line core and at the redward wing.

Now, most profile analyses so far concerning an isolated and saturated spectral line appear to have been generally involved with the latter type of microturbulence ($\xi_{\rm P}$). That is, a ξ value is chosen by the requirement of producing the best profile-fit, without any concern for the resulting abundance (even if it turned out to be unreasonable) necessary to be adjusted (corresponding to the adopted ξ) so as to reproduce the observed line-strength. This is because the main interest of such studies has been focused on establishing only the macroscopic velocity fields (e.g., rotation or macroturbulence) dominating the line-broadening, in which the intrinsic thermal profile plays merely the role of "marker for the Doppler shift" if we use the word of Gray (1988).

We stress here, however, that the microturbulence which we will refer to in this paper is that of the first type ($\xi_{\rm A}$), although our study is based on an isolated line-profile as in the case of the second-type analysis mentioned above. This is because it is requisite for us to establish the abundance of potassium in the Sun as precisely as possible, which directly affects the determinations of $\Delta \log C_6$ and $\zeta_{\rm RT}$ that we are aiming at, as well as because we are interested in the Procyon's K abundance relative to the Sun. In other words, our primary concern in the present profile analysis is to choose a ξ value which would yield a consistent potassium abundance.

From another point of view, this is equivalent to applying our MPF method while requiring that the solutions of the parameters should be subject to adequately formulated constraints corresponding to the conditions mentioned above. Accordingly, it should be kept in mind that the fit produced by our final solutions of the parameters may possibly be slightly worse than the best fit accomplished in the sense of the traditional profile-analysis where ξ is freely adjustable (i.e., the use of second-type ξ without any such restriction).

Practically, we decided to adopt a manual procedure in order to take this constraint into account in a reasonable way, such as was done in Paper IV. That is, we first applied the MPF method with various fixed values of ξ (and also of h in the case of the Sun) and prepared an ensemble of best-fit solutions for each of these prescribed parameters. We then selected from this solution space the most reasonable one matching the specified requirement. This procedure has a merit in that we can easily estimate the uncertainties of the solutions corresponding to the ambiguities in the demanded constraint. The details of how to arrive at the final solutions are more or less case-dependent, reflecting the difference in the available information, as elucidated in the following two subsections 4.4 (Sun) and 4.5 (Procyon). In any case, we again remark that our analysis is based on the fundamental

Table 1. Representative solutions of the parameters from the K I 7699 profile of the Sun.

ξ	h	log ϵ_K	ζ_{RT}	$\Delta \log C_6$	log f_c^{th}	σ
0.00	−3.0	5.34	2.84	+0.02	+0.0036	0.003085
0.00	−2.0	5.35	2.82	+0.01	+0.0038	0.003084
0.00	−1.0	5.45	2.70	−0.12	+0.0044	0.003082
0.00	0.0	5.69	2.09	−0.43	+0.0074	0.003200
0.25	−3.0	5.29	2.77	+0.15	+0.0039	0.003092
0.25	−2.0	5.31	2.75	+0.14	+0.0039	0.003091
0.25	−1.0	5.40	2.62	+0.02	+0.0047	0.003091
0.25	0.0	5.64	1.98	−0.28	+0.0077	0.003235
0.50	−3.0	5.16	2.54	+0.52	+0.0047	0.003109
0.50	−2.0	5.18	2.52	+0.51	+0.0047	0.003109
0.50	−1.0	5.28	2.37	+0.39	+0.0054	0.003118
0.50	0.0	5.51	1.57	+0.11	+0.0088	0.003398
0.75	−3.0	5.00	2.06	+1.03	+0.0061	0.003150
0.75	−2.0	5.01	2.03	+1.02	+0.0062	0.003155
0.75	−1.0	5.10	1.83	+0.91	+0.0070	0.003198
0.75	0.0	(5.34)	(0.34)	(+0.65)	(+0.0111)	(0.004793)
1.00	−3.0	4.82	0.98	+1.62	+0.0088	0.003468
1.00	−2.0	4.83	0.92	+1.61	+0.0090	0.003509
1.00	−1.0	(4.92)	(0.34)	(+1.50)	(+0.0090)	(0.004243)
1.00	0.0	...	...	...	...	...

Notes. See the text for the meanings of the quantities, though some are self-explanatory. The unit of ξ and ζ_{RT} is km s^{-1}. These solutions were obtained with a prescribed set of (ξ, h) which are shown in the 1st and 2nd columns, while the rotational velocity ($v_e \sin i$) was fixed at 1.90 km s^{-1} throughout. In all of the cases presented here, the parameter $\Delta\lambda_r$ has a converged solution of +0.007 Å. The acccuracy of the parenthesized values may be somewhat low, since iterations were stopped before reaching a complete convergence because the ζ_{RT} solution came outside of the parameter range of the $M(v)$ tabulation.

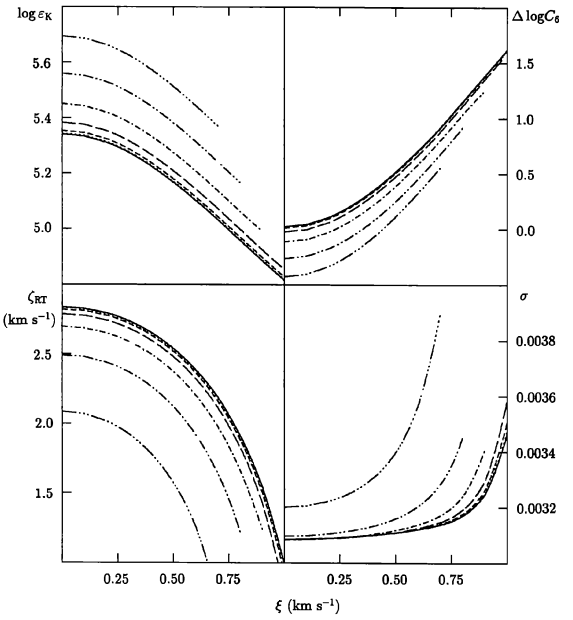

Fig. 5. Dependence of the converged solutions (log ϵ_K, ζ_{RT}, $\Delta \log C_6$, and the corresponding σ) upon the values of ξ and h, resulting from the profile analysis of K I 7699 in the solar flux spectrum based on Model-C. The solid line, dotted line, short-dashed line, long-dashed line, dash-dotted line, dash-double-dotted line, and the dash-triple-dotted line correspond to the h values of −3.0, −2.5, −2.0, −1.5, −1.0, −0.5, and 0.0, respectively.

principle of using ξ_A (the curve-of-growth-type microturbulence), putting the abundance-consistency in the first place.

4.4. *Results for the Sun*

Our analysis of the solar K I 7699 profile (described below) was based on Model-C, because the use of Model-E yields essentially the same results (cf. subsection 3.2). We assumed a fixed $v_e \sin i$ value of 1.9 km s^{-1}, which is regarded as being reasonable according to Paper III. It was also decided to apply the MPF method for evaluating only four parameters (log ϵ_K, ζ_{RT}, $\Delta\lambda_r$, and $\Delta \log C_6$) for various *given* combinations of (ξ, h), based on our strategy explained in the previous subsection. The finally converged results of log ϵ_K, ζ_{RT}, $\Delta \log C_6$, and the corresponding σ are graphically shown in figure 5, where each curve shows the run of the solution (for a specified value of h) in the range 0 km s^{-1} $\leq \xi \leq$ 1 km s^{-1}. The numerical values of the solutions for representative combinations of ξ and h are also presented in table 1, where $\Delta \log f_c$ is the logarithmic difference between the resulting theoretical continuum derived as a by-product and the empirically estimated continuum (i.e., $f_\lambda = 1$ level in the present case of normalized f_λ) (cf. subsection 6.6 of Paper III).

Our next task should be to choose the most adequate set of the solutions among these varieties. Following the guideline described in subsection 4.3 (i.e., ξ is so chosen as to yield the correct abundance), we required that (a) the resulting log ϵ_K solution be consistent with the mean abundance of 4.9–5.0 (being slightly h-dependent), which was averaged over those derived from the disk-center equivalent widths of seven weak lines (cf. table 2). Furthermore, since only this constraint on log ϵ_K is not sufficient to establish all of the variables concerned, we additionally postulate that (b) the ζ_{RT} value derived from

Table 2. Analysis of weak K I lines in the disk-center ($\mu = 1$) spectrum of the Sun.

RMT	l–u	λ(Å)	χ(eV)	$\log gf$	W_λ(mÅ)	$h=-3$	$h=-2$	$h=-1$	$h=0$	LTE	$\Delta_{\rm L1}$	$\Delta_{\rm A9}$	$\Delta_{\rm HM}$
(3)	1–5	4044.15	0.00	−1.91	11	4.85	4.86	4.88	4.92	4.94	−05	+03	+09
(3)	1–5	4047.23	0.00	−2.215	4	4.69	4.69	4.72	4.75	4.77	−05	+04	+09
(5)	2–3	12522.16	1.62	−0.136	54	4.83	4.84	4.88	4.94	4.96	−03	+06	+11
(–)	2–7	6938.74	1.62	−1.108	3	4.79	4.80	4.82	4.85	4.86	−03	+04	+07
(–)	2–11	5801.75	1.62	−1.61	1.5	5.04	5.05	5.07	5.09	5.10	−04	+04	+09
(–)	2–16	5339.70	1.62	−1.97	1	5.26	5.26	5.28	5.31	5.31	−04	+03	+06
(6)	2–4	11769.72	1.62	−0.444	33	4.93	4.93	4.98	5.02	5.04	−03	+04	+09
(–)	2–10	5831.94	1.62	−2.00	0.5	4.94	4.95	4.97	4.99	5.00	−03	+05	+10

Notes. The data in the 1st through 6th columns are the multiplet number (Moore 1959), the term combination, the wavelength, the lower excitation potential, the gf value (Wiese et al. 1969), and the equivalent width (taken from table XII of Lambert and Warner 1968), respectively. The resulting non-LTE abundances are shown in 7th through 10th columns corresponding to four different h-values, followed by the LTE abundance in the 11th column. The quantities $\Delta_{\rm L1}$, $\Delta_{\rm A9}$, and $\Delta_{\rm HM}$ denote the first two decimals of the abundance changes (relative to our standard case using Model-C) caused by the use of $l/H = 1$ (ATLAS6) model, ATLAS9 model (l/H=1.25), and Holweger and Müller's (1974) model, respectively. We assumed ξ= 1 km s^{-1} and $\Delta \log C_6$= 0 in deriving these abundances; at any rate, they are hardly affected by any choice of these parameters because of the weakness of these lines.

this line should be between 2.0 km s^{-1} and 2.5 km s^{-1} based on the empirical $\zeta_{\rm RT}$ vs. $\overline{\log\tau}$ relation depicted in figure 2 of Paper III. [The mean formation depth of this K I 7699 line (W_λ = 168 mÅ) was estimated to be $\overline{\log\tau} \simeq -2.1$ following the same way as in subsection 5.1 of Paper III.]

With the help of these requirements (a) and (b), we can settle all of the parameters by inspecting figure 5 in a reasonable way (as described below).

— The condition of $\log\epsilon_{\rm K} \simeq$ 4.9–5.0 implies that $\xi \simeq$ 0.8–0.9 km s^{-1} for $(-\infty <)h \lesssim -2$ (the results are almost h-independent in the case of $h \lesssim -2$ where finding an exact h value is neither possible nor meaningful; cf. subsection 3.2), while the corresponding ξ value becomes systematically *larger* as h is increased from about −2 to a larger value.

— The requirement of 2.0 km s$^{-1} \lesssim \zeta_{\rm RT} \lesssim$ 2.5 km s^{-1} suggests that 0.5 km s$^{-1} \lesssim \xi \lesssim$ 0.8 km s^{-1} for $(-\infty <) h \lesssim -2$, while the corresponding ξ range systematically shifts to *smaller* values along with an increase of h (from about $h \simeq -2$ toward larger).

— It is then easy to see that the combination of (h, ξ) satisfying these two conditions must be almost uniquely restricted to $(-\infty <)h \lesssim -2$ and $\xi \simeq$ 0.8 km s^{-1}.

— With this choice of h and ξ, the remaining parameters are finally read from figure 5 as $\log\epsilon_{\rm K} \simeq$ 5.0, $\zeta_{\rm RT} \simeq$ 2.0 km s^{-1}, and $\Delta \log C_6 \simeq +1.0$.

We regard these as being the best solutions of the parameters to be adopted, which were derived from the profile of K I 7699 in the solar flux spectrum. The theoretical profile corresponding to these parameters are compared with the observed data in the left-hand panel of figure 6, where we can recognize a nearly perfect fit.

The constraints on $\log\epsilon_{\rm K}$ and $\zeta_{\rm RT}$ used in the above discussion are subject to internal errors of $\delta\log\epsilon_K \sim \pm 0.1$ dex and $\delta_{\rm RT} \sim \pm 0.2$ km s^{-1}. Thus, the relation $\delta\xi \simeq (\partial\xi/\partial\log\epsilon_{\rm K})\delta\log\epsilon_{\rm K} + (\partial\xi/\partial\zeta_{\rm RT})\delta\zeta_{\rm RT}$, where the partial derivatives around the fiducial solutions can be estimated from figure 5, indicates that the key-parameter ξ has an uncertainty amounting to $\sim \pm 0.2$ km s^{-1}. This further suggests that the internal error of $\Delta \log C_6$ would be $\sim \pm 0.4$ dex according to figure 5; but the conclusion of $h \lesssim -2$ remains unaltered, even when such ambiguities of the solutions are taken into consideration.

Finally, it should be noted that the smallest σ in the strict sense (among all possible cases shown in table 1) is attained at $\xi = 0$ km s^{-1} ($\xi_{\rm P}$; though it yields evidently unreasonable abundance). Such a possibility was already mentioned in subsection 4.3; the reason will be discussed in subsection 5.1.1.

4.5. Results for Procyon

Regarding the K I 7699 analysis of Procyon, which is based on Model-P, we first prepared a grid of solutions for various given values of ξ, following the strategy described in subsection 4.3. In doing so, we made use of the results for the Sun by assuming $h = -3.0$ (i.e., H I collisions being practically neglected) and $\Delta \log C_6 = +1.0$ as being fixed, whereas $v_{\rm e} \sin i$ is yet to be determined in this case. Accordingly, the parameters to be evaluated by applying the MPF method in setting up the grid are $\log\epsilon_{\rm K}$, $\zeta_{\rm RT}$, $v_{\rm e} \sin i$, and $\Delta\lambda_{\rm r}$. The resulting solutions for a set of ξ values ranging from 0 km s^{-1} to 2 km s^{-1} are presented in table 3.

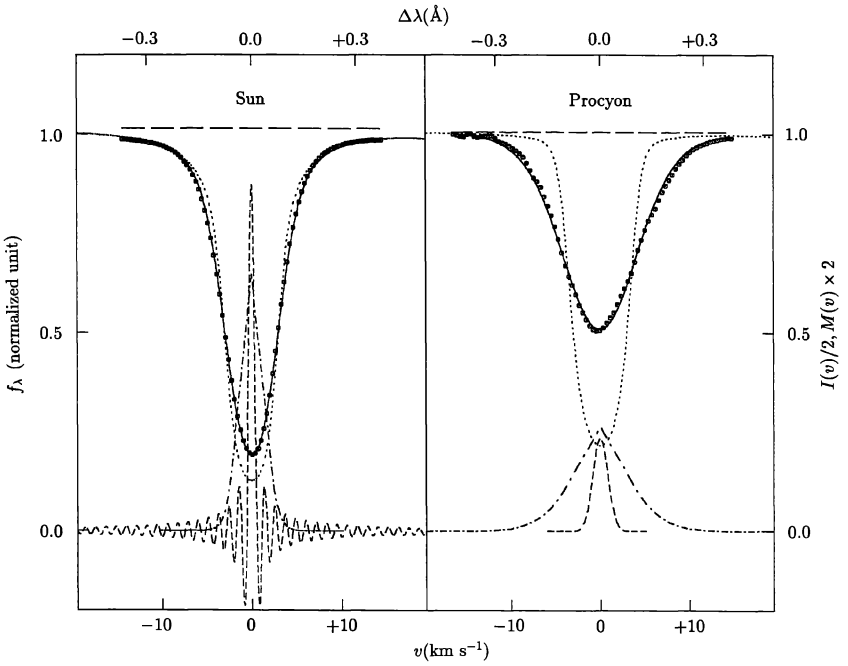

Fig. 6. Fitting appearance of the theoretical profiles (corresponding to nearly the most appropriate solutions of the parameters) with the observed ones. The left-hand panel shows the case for the Sun [Model-C; $\xi = 0.75$ km s^{-1} and $h = -3.0$ (cf. table 1)], while the right-hand one is for Procyon [Model-P; $\xi = 1.50$ km s^{-1} and $h = -3.0$ (cf. table 3)]. The observed data are shown by symbols (circles), while the solid line, dotted line, short-dashed line, and the dash-dotted line represent the finally convolved profile (to be compared with observation), the intrinsic profile before being convolved, the instrumental profile [$I(v)$], and the macrobroadening function [$M(v)$], respectively. The long-dashed line indicates the theoretically evaluated continuum position, which is irrespective of the empirically estimated level used for the normalization. See also the caption of Paper III's figure 1.

Our task is now to choose the most reasonable solution from this table. Unfortunately, unlike in the case of the Sun, we can not settle the microturbulence directly by means of constraining the abundance, because the weak subordinate lines of potassium (which could be used to restrict the abundance scale in the solar case) are too weak to be measured and are no longer available. Hence, we have to find and invoke some other remedy for this case. Keeping the principle in mind that we should use the conventional curve-of-growth-type microturbulence (ξ_A; according to the definition in subsection 4.3), we decided to rely upon the information on ξ_A independently determined from the equivalent widths of iron-group lines, the procedures of which are described in appendix 2. As shown in figure 9 therein, this parameter was found to be depth-dependent. Considering that the mean-formation-depth for this case is estimated to be $\overline{\log \tau} \sim -1.6$, we tentatively assume $\xi \simeq 1.4$ km s^{-1} from this figure. Then, table 3 yields $\log \epsilon_K \simeq 5.0$, $\zeta_{RT} \simeq 6.7$ km s^{-1}, and $v_e \sin i \simeq 3.3$ km s^{-1} as the most reasonable solutions of the parameters. How the theoretical profile corresponding to these results fits the observed one is depicted in the right-hand panel of figure 6. It is interesting to note that this choice of $\xi \simeq 1.4$ km s^{-1} fortuitously corresponds to the smallest σ among all possibilities in table 3. This situation ($\xi_A \simeq \xi_P$) is different from the solar case ($\xi_A > \xi_P$) mentioned before.

By the way, in order to examine the significance/insignificance of the hand-correction applied to remove the unreasonable distortion of the profile (cf. subsection 4.1), we also performed a test calculation for the representative $\xi = 1.5$ km s^{-1} case by using the *uncorrected* raw spectra, and obtained ($\log \epsilon_K$, ζ_{RT}, $v_e \sin i$, $\Delta\lambda_r$) = (4.95, 7.6 km s^{-1}, 1.7 km s^{-1}, 0.15 Å). By comparing these values with the corresponding standard ones presented in table 3 (4.94, 6.7 km s^{-1}, 3.2 km s^{-1}, 0.15 Å), we can see how the resulting solutions are sensitive to applying this correction; i.e., a significant change is observed only in $v_e \sin i$ which has a comparatively minor contribution to the total line-broadening.

Table 3. Converged solutions of the parameters from the K I 7699 profile of Procyon.

ξ	h	$\log \epsilon_K$	ζ_{RT}	$v_e \sin i$	$\log f_c^{th}$	σ
0.00	−3.0	5.35	6.05	4.38	+0.0032	0.004783
0.25	−3.0	5.33	6.08	4.36	+0.0032	0.004782
0.50	−3.0	5.28	6.18	4.25	+0.0030	0.004779
0.75	−3.0	5.21	6.30	4.11	+0.0028	0.004774
1.00	−3.0	5.12	6.44	3.88	+0.0025	0.004768
1.25	−3.0	5.03	6.58	3.58	+0.0024	0.004764
1.50	−3.0	4.94	6.71	3.18	+0.0023	0.004763
1.75	−3.0	4.86	6.82	2.66	+0.0022	0.004769
2.00	−3.0	4.79	6.89	1.97	+0.0020	0.004788
2.25	−3.0	4.73	6.85	0.98	+0.0015	0.004830

Notes. The unit of ξ, ζ_{RT}, and $v_e \sin i$ is km s^{-1}. The listed solutions, all corresponding to $h = -3$, were obtained with each prescribed value of ξ (1st column). In all of the cases presented here, the parameter $\Delta\lambda_r$ has a converged solution of +0.150 Å.

5. Discussion

5.1. *Implications from the Sun*

5.1.1. *Microturbulence problem*

We found from analysis of the solar K I 7699 profile (cf. subsection 4.4) an evident discordance between two kinds of microturbulences derived from different approaches. That is, while the smallest σ (i.e., the best fitting) among all possible cases is accomplished by the choice of $\xi \simeq 0$ km s^{-1}, we had to adopt $\xi \simeq 0.8$ km s^{-1} in order to obtain a reasonable abundance that is consistent with those resulting from weak lines. In other words, the profile-based microturbulence (ξ_P; determined from the degree of boxiness at the core of a saturated line) is apparently smaller than the conventionally established ξ value (ξ_A; which is based on the requirement of abundance consistency between the lines on the linear and the flat part of the curve of growth). Interestingly, such a tendency (though to a lesser extent) had also already been noticed in Paper III (see subsection 6.1 therein). What would be the reason for this discrepancy?

Here, it is worth recalling that the latter conventional approach makes use of the strong ξ-dependence of the abundance derived from a saturated line, for which the relation $W_\lambda (\simeq R_0 \Delta\lambda_D) \propto \Delta\lambda_D$ ($\Delta\lambda_D$: Doppler width of the line opacity determined by ξ) almost holds because the line depth (R_0) is insensitive to ξ (unlike the case of weak lines where W_λ is independent of $\Delta\lambda_D$ because $R_0 \propto \Delta\lambda_D^{-1}$); this means that such a determined ξ reflects the extent of $\Delta\lambda_D$ (i.e., microscopic Doppler motion) at the line-forming depth of $\tau_\nu \sim 1$, corresponding to the profile point (ν) where the half-width is measured (i.e., $R_\nu \simeq R_0/2$). Meanwhile, the microturbulent velocity determined by the former approach (invoking the core-shape) is expected to reflect $\Delta\lambda_D$ at the region of core-photon formation; this depth should naturally be higher than that described just above. Taking all of these facts into consideration, we may speculate as a possibility that ξ decreases along with an increase in the atmospheric height in the considered region of the solar photosphere, which may explain the above-mentioned discordance of ξ. Since this implies that the depth-dependence of ξ is qualitatively similar to that of ζ_{RT} (cf. subsection 6.2 of Paper III), they may presumably be closely related with each other. It is likely that both of these two kinds of turbulences may be associated with the convective granular motions, which are known to be decelerating upwards.

We further suspect that this behavior of ξ, decreasing with height, is a common characteristics which generally holds in the atmospheres of solar-type (F–G) stars, as supported by evidence for the case of Procyon (cf. appendix 2) showing the same trend (yet, why then $\xi_A \simeq \xi_P$ holds for this star, unlike the in solar case, still remains as a meaningful question). It should be kept in mind, however, that this tendency is apt to be reversed for stars of different types, especially for low-gravity stars, such as in the case of the K giant Arcturus (cf. Takeda 1992) or A–F supegiants (cf. Takeda and Takada-Hidai 1994), for which ξ was found to increase outwards in their atmospheres.

5.1.2. *H I collision rates*

We found in subsection 4.4 that the parameter h (controlling the H I collisions), determinable from the solar K I 7699 profile, should fall within the range of $-\infty < h \lesssim -2$, which means that the effect of neutral-hydrogen collisions is practically negligible in the rate equations because $C_H(1C)$ [$\lesssim 10^2 C_e(1C)$], calculated by the standard formula, should be multiplied by a reduction factor amounting to $\lesssim 10^{-2}$ (or even further less). Since it was impossible to specify an exact value of h within this range (any choice can do), we tentatively assigned $h = -3$, which has been used for the K I 7699 analysis of Procyon.

It should be remarked here that this result is markedly different from what was found in Paper VI, where we concluded that $h \simeq 0$ (from O I 7771–5) and $h \simeq -1$ (from Na I 8183/95) based on profile analyses of these lines in the solar flux spectrum. Accordingly, we must regard that the situation concerning how to treat H I collisions strongly depends on the lines and/or species, which should be investigated case by case.

Though neither theoretical nor experimental evaluations of C_H for K I transitions are available to our knowledge, several recent results of atomic physics suggest that the H I collision rates calculated by the standard formula [such as adopted for $C_H(1C)$] are drastically overesti-

mated by orders of magnitude for the resonance transition of Li I (2s ^{2}S–2p ^{2}P) and Na I (3s ^{2}S–3p ^{2}P), as reviewed by Lambert (1993) (see also Caccin et al. 1993). If we assume that these results can also be applied to our present case of K I 7699, because of being a similar alkali resonance line, our consequence of setting $h \lesssim -2$ may be regarded as being consistent with those implications from the side of atomic physics.

We also note, based on the results of our empirical h values determined so far, that there seems to exist a dependence of h upon the excitation potential; i.e., $h \simeq 0$ for the high-excitation lines (O I 7771–5), $h \simeq -1$ for the low-excitation lines (Na I 8183/95) and $h \lesssim -2$ for the resonance line (K I 7699). This is an interesting tendency (though its generality is yet to be confirmed), which might be used for a rough estimate of this parameter in various other cases.

5.1.3. *Damping constant*

Our analysis of the solar K I 7699 profile suggested that $\Delta \log C_6 \simeq +1.0$, which means that the damping width [$\Gamma_6 (\propto C_6^{2/5})$] computed using Unsöld's (1955) classical formula should be multiplied by a factor of ~ 2.5. We must recall, however, that an empirical determination of this parameter sensitively depends on the choice of the model atmosphere, as shown for the case of sodium lines in Paper IV. If we use Holweger and Müller's (1974) empirical solar model, for example, which may represent the photospheric temperature structure better than Kurucz's (1979) theoretical model (cf. subsection 5.3.1) adopted by us, we obtain an appreciable increase (by $\sim +0.4$) in this parameter, resulting in $\Delta \log C_6 \simeq +1.4$. Hence, our empirical values should be regarded as being involved with such ambiguities, though they do suggest the necessity of an appreciable enhancement to the classical value. Meanwhile, Andretta et al.'s (1991) theoretical calculation indicates that $\Delta \log C_6 \simeq +0.6$ (corresponding to the enhancement factor of ~ 1.7 they derived) for this K I 7699 line, which appears to be somewhat small compared to our empirical estimation (described above). In any case, we may reasonably conclude that $\Delta \log C_6 \simeq +1.0$ with an uncertainty of $\sim \pm 0.4$ (which is the same extent as the internal error estimated in subsection 4.4) from these considerations, which has been adopted as the standard value in this paper.

Finally, one remark may be due regarding the work of Bruls and Rutten (1992), who tried to fit the K I 7699 profile by using $\Delta \log C_6 = 0$ (see figure 18 therein). It may be pointed out, however, that their modeling does not appear to be very reliable, at least in the quantitative sense, in spite of their qualitative success in reproducing the observed asymmetry. That is, as can be seen from their figure 18, the Na I D_1 profile computed by them is too wide (even by using $\Delta \log C_6 = 0$) compared to the observed profile; this indicates that they would require a negative $\Delta \log C_6$ value so as to fit this sodium resonance line, which is hardly acceptable in view of the published theoretical results ($\Delta \log C_6 \sim +0.5$; see subsection 4.2 of Paper IV). Based on this fact that the profile calculated by them tends to be too strong, their fit of the K I 7699 width with $\Delta \log C_6 = 0$ would naturally suggest that the true value of this correction for this potassium line should actually be positive.

5.2. *Procyon's Velocity Fields*

5.2.1. *Comparisons with previous works*

We now discuss how the atmospheric velocity-parameters of Procyon ($\xi \simeq 1.4$ km s^{-1}, $\zeta_{\rm RT} \simeq 6.7$ km s^{-1} and $v_{\rm e} \sin i \simeq 3.3$ km s^{-1}) established in subsection 4.5 compare with the available published values. To our knowledge, there have been three different profile-analyses based on the Fourier-transform method, which were carried out by Wynne-Jones et al. (1978), Gray (1981), and de Jager and Neven (1982).

Among these, special attention should be paid in the first place to the work of Gray (1981), because it was based on the same macroturbulence broadening function (i.e., the radial-tangential form) as that adopted in this study, and (thus) both results may be directly compared with each other. However, the line-dependent ξ values assigned by Gray (1981) (which tend to increase with the lower excitation potential in the range of 0–3 km s^{-1}) have little meanings in the absolute sense because of the uncertainties in the "zero-point"; namely, his analysis was conducted basically with an assumed ξ value of 0 km s^{-1} (i.e., no interest for abundance determination) which was then arbitrarily increased (if necessary) so as to remove the line-dependence of $\zeta_{\rm RT}$ (we feel that this requirement may be somewhat questionable in view of the evidence of depth-increasing $\zeta_{\rm RT}$ in the solar atmosphere; cf. Paper III). Yet, its qualitative tendency, which he found, is consistent with our conclusion that ξ increases with depth (appendix 2), and (in any case) the uncertainties in the ξ values do not seriously affect the determinations of $\zeta_{\rm RT}$ and $v_{\rm e} \sin i$ because of its minor contribution to the total line broadening. We can thus see that his results ($\zeta_{\rm RT} = 7.0$ km s^{-1}, $v_{\rm e} \sin i = 2.8$ km s^{-1}) are in good agreement with ours ($\zeta_{\rm RT} = 6.7$ km s^{-1}, $v_{\rm e} \sin i = 3.3$ km s^{-1}); this assures the reliability of these solutions derived from both independent analyses, which were based on different methods as well as on different observational materials.

Regarding the other two studies, it is not very meaningful to discuss their results in comparison with our solutions, since they adopted their own macroturbulence functions, which are considerably different from ours. Still, some remarks may be due.

Wynne-Jones et al. (1978) derived from the profile of

Fe II λ4924 $\xi = 2.5$ km s^{-1}, $\zeta_e = 0.75$ km s^{-1} (exponential form), and $v_e \sin i = 3.5$ km s^{-1}. Disregarding the ζ value (which appear to be too small) for the reason mentioned above, we may regard their solutions of ξ and $v_e \sin i$ as being reasonable; this seemingly somewhat large ξ value may be due to the fact that the Fe II line is formed deep in the atmosphere where the relevant ξ is correspondingly large (cf. figure 9).

Meanwhile, de Jager and Neven (1982) studied the profiles of two UV lines (Fe III λ2137.2 and Si I λ2081.8) with two kinds of macroturbulance broadening functions (i,e., sinusoidal and Gaussian). They obtained $\xi = 0.9$ km s^{-1}, ($v_e \sin i = 10.0$ km s^{-1}, $\zeta_s = 5.3$ km s^{-1}) for the sinusoidal form of macroturbulence, and ($v_e \sin i = 4.0$ km s^{-1}, $\zeta_G = 11.6$ km s^{-1}) for the Gaussian form. Since these ($v_e \sin i$, ζ) solutions are sensitively dependent upon the choice of the macroturbulence form, the appreciable discrepancies compared to our results should not be of too much concern. The notable smallness of their ξ value might be interpreted by the fact that the formation-depth of such UV lines is generally high, where the corresponding ξ should naturally be small, according to its depth-dependence.

5.2.2. *Radial velocity*

We obtained +0.150 Å as the solution of the wavelength shift ($\Delta\lambda_r$) from our MPF analysis of K I 7699 (see the notes in table 3), which yields V_r(topo) = +5.84 km s^{-1} as the topocentric radial velocity at the observational time. With the correction of -8.23 km s^{-1}, the heliocentric radial velocity turns out to be V_r(helio) = -2.4 km s^{-1}. Meanwhile, the predicted V_r(helio) value of Procyon (constituting a visual binary system with a white-dwarf companion) was calculated to be -3.3 km s^{-1} according to the orbital elements presented by Hirshfeld and Sinnott (1985). We may then regard that both V_r(helio) values are in tolerable agreement with each other.

It should also be pointed out, in addition, that our K I 7699 profile of Procyon shows an appreciable asymmetry (see figures 4 and 6), which is a real effect generally observed in the line profiles of this star (cf. figure 18.16 of Gray 1992). Thus, some uncertainties caused by our attempt to fit the intrinsically asymmetric line with a symmetric theoretical profile would be inevitable in our V_r results. Interestingly, the radial velocity measured at the *bottom* of the profile (at $\sim$ 7699.10 Å; see figure 4), which is about ~ 1 km s^{-1} smaller than the value mentioned above (as can be estimated also from figure 6), now turns out to agree with the predicted V_r almost exactly.

Table 4. Solar potassium abundance from the flux equivalent width of K I 7699.

	$h=-3$	-2	-1	0	$+\infty$(LTE)
$\Delta \log C_6 = +1.0$					
$\xi = 0.8$ km s^{-1}	4.91	4.92	4.97	5.09	5.27
$\xi = 1.0$ km s^{-1}	4.88	4.88	4.94	5.06	5.24
$\Delta \log C_6 = +0.6$					
$\xi = 0.8$ km s^{-1}	5.01	5.02	5.07	5.19	5.40
$\xi = 1.0$ km s^{-1}	4.96	4.97	5.03	5.15	5.37

(Abundance changes due to the use of different model atmospheres.)

-0.03 $l/H = 1$ ATLAS6 model (5770, 4.44, 1.0)
+0.16 Holweger and Müller's (1974) model (5780, 4.44, 1.0)
+0.06 ATLAS9 model (5777, 4.438, 1.25)

Notes. As in our previous papers (e.g., Takeda 1992b), the abundance variations were estimated by LTE calculations; i.e., relative to the LTE solution based on our reference Model-C [practically equivalent to the ATLAS6 model of (5770, 4.44, 2.0)], corresponding to the finally adopted standard condition ($\Delta \log C_6 = +1.0$ and $\xi = 0.8$ km s^{-1}).

5.3. *Potassium Abundance*

To conclude this paper, we discuss the non-LTE potassium abundances for the Sun and Procyon which were derived from the K I 7699 line, clarifying how they are affected by changing the parameters or model atmospheres. For convenience, our discussions are mainly based on the results derived from the equivalent widths.

5.3.1. *log ϵ_K (Sun)*

Table 4 shows how the solar potassium abundance, conventionally derived from the (flux) equivalent width of K I 7699 ($W_\lambda = 168$ mÅ; measured from the observational data adopted in this study), depends upon the atomic parameters (h, $\Delta \log C_6$), the microturbulence, and the adopted model atmosphere. For our standard choice of those parameters ($\xi = 0.8$ km s^{-1}, $h = -3$, $\Delta \log C_6 = +1.0$) on Model-C, we see $\log \epsilon_K = 4.91$ from this table, which is consistent with the averaged abundance of 4.92 ($\pm$0.16) ($h = -3$) determined from weak lines (cf. table 2).

It should be taken into account here that Holweger and Müller's (1974) empirical model appears to represent the solar photospheric temperature structure more correctly than do such theoretical models as that of Kurucz (1979) adopted as our reference model (see, e.g., Blackwell et al. 1995, Holweger et al. 1995). Thus, by applying a corresponding correction of +0.16 (taken from table 4), we obtained $\log \epsilon_K$(Sun) $\simeq$ 5.1 as the solar potassium

Table 5. Potassium abundance of Procyon from the equivalent width of K I 7699.

	$h=-3$	-2	-1	0	$+\infty$(LTE)
$\Delta\log C_6=+1.0$					
$\xi=1.4$ km s^{-1}	4.98	4.98	5.02	5.21	5.66
$\xi=2.0$ km s^{-1}	4.80	4.80	4.85	5.02	5.47
$\Delta\log C_6=+0.6$					
$\xi=1.4$ km s^{-1}	5.00	5.01	5.05	5.24	5.74
$\xi=2.0$ km s^{-1}	4.81	4.82	4.86	5.04	5.52

(Abundance changes due to the use of different model atmospheres.)

-0.03	$l/H=1$ ATLAS6 model (6500, 4.0, 1.0)
$+0.37$	$\Delta T_{\rm eff}=+500$ ATLAS6 model (7000, 4.0, 2.0)
$+0.14$	$\Delta\log g=-0.5$ ATLAS6 model (6500, 3.5, 2.0)
$+0.08$	ATLAS9 model (6500, 4.0, 1.25)
$+0.29$	ATLAS9 model (6750, 4.0, 1.25)

Notes. The listed abundances were derived based on our reference Procyon model [ATLAS6 model of (6500, 4.0, 2.0)], relative to which the effects of different model atmosphere were estimated as in table 4 (with respect to the adopted standard condition of $\Delta\log C_6=+1.0$ and $\xi=1.4$ km s^{-1}).

abundance determined from W_λ(K I 7699), which is in agreement with the photospheric/meteoric abundance of 5.12/5.13 presented in the compilation of Anders and Grevesse (1989).

5.3.2. $\log\epsilon_K$ (Procyon)

The dependences of Procyon's $\log\epsilon_{\rm K}$, derived from the equivalent width of K I 7699 ($W_\lambda=138$ mÅ; measured from our observational data), upon the various parameters or the model atmospheres are presented in table 5. We can see from this table that $\log\epsilon_{\rm K}=4.98$ for our standard choice of the parameters ($\xi=1.4$ km s^{-1}, $h=-3$, and $\Delta\log C_6=+1.0$) on Model-P, which is essentially the same as that from our profile analysis based on the MPF method.

A considerably large extent of the (negative) non-LTE correction (-0.7 dex), which is defined as $\log\epsilon$ ($h=-3$)$-\log\epsilon$ ($h=+\infty$), is worth noting. We may thus conclude that the assumption of LTE is evidently inadequate for the abundance determination from this line; even a differential LTE analysis relative to the Sun would result in a significant error, since the amount of corrrection is appeciably different from that for the solar case (-0.4 dex; cf. table 4).

As shown in appendix 1, the best Procyon model is regarded as being the ATLAS6 model with parameters of $T_{\rm eff}\simeq6600$ K and $\log g\simeq3.9$ (corresponding to the $l/H\sim1$, though its role is insignificant). Therefore, a small correction amounting to $\sim+0.1$ dex (corresponding to $\Delta T_{\rm eff}=+100$ K and $\Delta\log g=-0.1$; estimated from table 5) may as well be applied to the $\log\epsilon_{\rm K}$ value based on our standard model. Hence, we conclude that $\log\epsilon_{\rm K}$(Procyon) $\simeq5.1$, confirming that the photospheric potassium abundance of this star is essentially the same as that of the Sun.

We wish to thank Dr. R. L. Kurucz for kindly sending us a CD-ROM set containing the solar flux spectrum and the ATLAS9 model fluxes, of which we made use in this study.

The computations were performed on FACOM M780/10S at the Astronomical Data Analysis Center of the National Astronomical Observatory.

Appendix 1. On the Model Atmosphere of Procyon

In connection with the present study, we tried to reinvestigate the problem regarding the choice of the most appropriate model atmosphere of Procyon, in the sense that the computed theoretical flux shows the best fit with the observed energy distribution. It is easily noticed that our MPF method is quite suitable for this purpose (i.e., simultaneous determinations of model parameters), which we decided to apply.

We regard the logarithmic theoretical flux as being a function of $T_{\rm eff}$ and $\log g$ as $\log F_\lambda(T_{\rm eff},\log g)$, which we express in an explicit analytical form by using the $\log F_\lambda$'s of the four basic "pole" models [such as was done by Takeda (1994b); cf. equation (1) therein] so as to enable quick computations of $\partial\log F_\lambda/\partial T_{\rm eff}$ and $\partial\log F_\lambda/\partial\log g$. Regarding the (absolutely calibrated) observed flux distribution (f_λ) of Procyon, we invoked that published by Kiehling (1987), in which those data marked with colons in his table 2 as being unreliable, as well as those coinciding with strong absorption features, were discarded. In addition, we introduced λ-dependent weights proportional to $F_\lambda/F_{\rm c}$ in the evaluation of σ (cf. subsection 5.3 of Paper I), thus putting larger weights on the continuum energy distribution.

The resulting converged solutions of $T_{\rm eff}$ and $\log g$ are presented in table 6, each of which are based either on the newly calculated models by using the ATLAS6 program (Kurucz 1979) with various l/H values (from 0.0 to 2.0), or on the more updated ATLAS9 models computed with $l/H=1.25$ (Kurucz, private communication, CD-ROM No.13). Figure 7 shows the appearance of the fit for the representative cases, achieved with the use of F_λ corresponding to the resulting solutions of $T_{\rm eff}$ and $\log g$. In table 6 are also presented the relevant values of the photometric angular diameter $\theta_{\rm ph}$ [$\propto(f_\lambda/F_\lambda)^{1/2}$], which were naturally derived as by-products of this MPF

Table 6. Effect of convection mixing length upon the photometric determination of $T_{\rm eff}$ and $\log g$.

Model	l/H	$T^0_{\rm eff}/T^1_{\rm eff}$	$\log g^0/\log g^1$	$T_{\rm eff}$	$\log g$	$\theta_{\rm ph}$	σ
ATLAS6	0.00	6000/6500	3.5/4.0	6523	4.044	5.535	0.00625
ATLAS6	0.25	6000/6500	3.5/4.0	6529	4.026	5.526	0.00627
ATLAS6	0.50	6000/6500	3.5/4.0	6542	3.995	5.501	0.00641
ATLAS6	0.75	6500/7000	3.5/4.0	6565	3.979	5.470	0.00665
ATLAS6	1.00	6500/7000	3.5/4.0	6581	3.943	5.443	0.00683
ATLAS6	1.25	6500/7000	3.5/4.0	6596	3.908	5.418	0.00702
ATLAS6	1.50	6500/7000	3.5/4.0	6611	3.878	5.393	0.00717
ATLAS6	1.75	6500/7000	3.5/4.0	6624	3.846	5.371	0.00731
ATLAS6	2.00	6500/7000	3.5/4.0	6635	3.815	5.349	0.00745
ATLAS9	1.25	6500/7000	3.5/4.0	6771	4.055	5.105	0.00858

Notes. The 1st through 4th columns describe the basic "pole" models used for interpolation (cf. Takeda 1994b), while the resulting best-fit parameters and the σ values are given in the 5th through 8th columns. The units of $T_{\rm eff}$, $\log g$, and $\theta_{\rm ph}$ (photometric angular diameter directly related to the offset constant C) are K, cm s^{-2}, and mas, respectively.

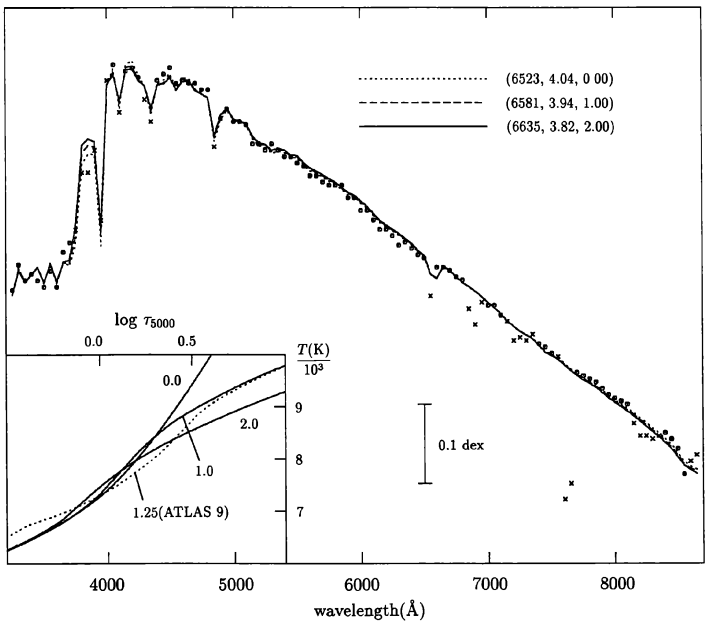

Fig. 7. Main figure: Comparison of the observed energy distribution of Procyon with the theoretical ones corresponding to the most adequate ($T_{\rm eff}$, $\log g$) combination determined on ATLAS6 models for $l/H = 0$ (dotted line), 1 (dashed line), and 2 (solid line) (cf. table 6). Both fluxes are adjusted with each other according to the converged offset constant C (equivalent to $\theta_{\rm ph}$ given in table 6). The observational data from Kiehling (1987) are shown by symbols (o ··· adopted data for the $T_{\rm eff}/\log g$ determination, × ··· excluded data because of being contaminated or less accurate).
Inset: The temperature distributions around $\tau_{5000} \sim 1$ for four different models having the same ($T_{\rm eff}$, $\log g$) of (6500, 4.0). Solid lines — ATLAS6 models with l/H=0, 1, and 2; dotted line ··· ATLAS9 model with $l/H = 1.25$.

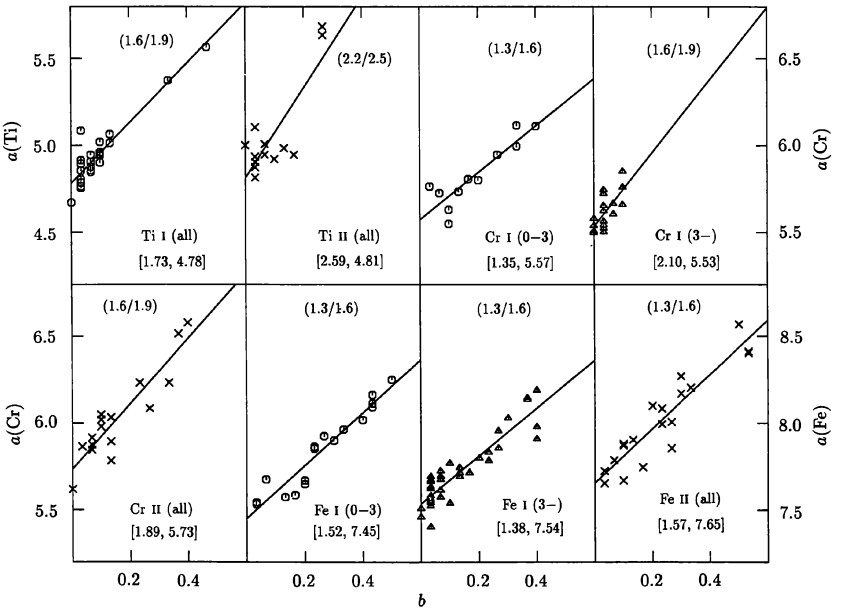

Fig. 8. Two-dimensional display of the (a, b) values derived by applying the ξ-determination method of de Jager et al. (1984) to Procyon, while based on Model-P and the equivalent-width data of Ti I/II, Cr I/II, and Fe I/II lines taken from Kato and Sadakane's (1982) table 4. The notation $(p$–$q)$ after the species name denotes the range of the lower excitation potential as $p \leq \chi(\mathrm{eV}) < q$. The linear regression line, $a = \xi b + \log \epsilon$, determined by a least-squares fit, is depicted by the solid line in each figure, where the adopted (ξ_1/ξ_2) values (cf. Takeda 1992) and the resulting values of $[\xi, \log \epsilon]$ are also indicated.

analysis from the converged C values. The following conclusions can be drawn by inspecting this table.

Regarding the ATLAS6 models, the results are insensitive to any choice of l/H, reflecting the fact that the effect of changing l/H upon $T(\tau)$ becomes conspicuous only at a fairly deep region of the atmosphere ($\log \tau_{5000} \gtrsim 0.2$; see the inset in figure 7). Thus, we may simply average the solutions for the two cases of $l/H = 0$ and 2 in order to obtain an estimate, which yields $T_{\mathrm{eff}} = 6579 \pm 56$ K, $\log g = 3.930 \pm 0.115$, and $\theta_{\mathrm{ph}} = 5.442 \pm 0.093$ mas. Note that this photometric θ_{ph} value is in fairly good agreement with the directly measured angular diameter of 5.50 ± 0.17 mas. (Hanbury Brown et al. 1974).

Meanwhile, the solutions ($T_{\mathrm{eff}} = 6771$ K, $\log g = 4.055$) derived from the ATLAS9 models indicate an appreciably higher T_{eff} and a slightly larger $\log g$ (i.e., $\Delta T_{\mathrm{eff}} \simeq +200$ K and $\Delta \log g \simeq +0.15$ compared to the ATLAS6 case), which is due to the significantly smaller temperature gradient at the continuum forming region (cf. the inset in figure 7). Thus, the recent finding of Gerbaldi et al. (1995), who noticed a significant T_{eff}-discrepancy for this star between that derived from the ATLAS6 colors through the use of Moon and Dworetsky's (1985) calibration ($T_{\mathrm{eff}} = 6570$ K) and that based on the ATLAS9 colors ($T_{\mathrm{eff}} = 6820$ K), has been reasonably confirmed.

Thus, a question would naturally be asked, "which solution should we adopt, ATLAS6 or ATLAS9 ?". Our answer is that the former (ATLAS6) is preferable to the latter, because the resulting θ_{ph} value (5.105 mas) in the ATLAS9 case is in apparent conflict with the direct measurement quoted above, contrary to the case of ATLAS6 models where the agreement was quite satisfactory. Though this is a rather unexpected result, which one might feel reluctant to accept, we would conclude the preference of the old ATLAS6 models (as far as the present case of Procyon is concerned), suspecting that the treatment of convection in the new ATLAS9 program may not be quite adequate.

Consequently, our recommended model atmosphere for Procyon is the ATLAS6 model with $T_{\mathrm{eff}} \simeq 6600$ K and $\log g \simeq 3.9$, where the involved uncertainties due to the ambiguities in the l/H values (any choice between 0 and 2 can produce a sufficiently good fit) are $\lesssim 100$ K and ~ 0.1, respectively. We finally point out that equation (3) of Takeda and Takada-Hidai (1994), a useful formula for estimating the mass of A–F stars, yields $M \simeq 1.8\ M_{\odot}$ for this combination of T_{eff} and $\log g$, which just agrees with the value ($M = 1.76 \pm 0.10\ M_{\odot}$) derived from the

Table 7. Model-dependence of the ionization equilibria of Ti, Cr, and Fe in Procyon.

Model	($T_{\rm eff}$, $\log g$, l/H)	ξ	Ti I(25)	Ti II(13)	Cr I(29)	Cr II(16)	Fe I(55)	Fe II(20)
ATLAS6	(6500, 4.0, 2.00)	1.5	4.80(±0.07)	4.94(±0.20)	5.55(±0.08)	5.80(±0.11)	7.50(±0.08)	7.67(±0.10)
		2.0	4.76(±0.07)	4.87(±0.16)	5.51(±0.09)	5.72(±0.10)	7.43(±0.11)	7.58(±0.11)
ATLAS6	(7000, 4.0, 2.00)	1.5	5.18(±0.10)	5.07(±0.22)	5.85(±0.10)	5.80(±0.11)	7.82(±0.09)	7.71(±0.10)
		2.0	5.14(±0.09)	5.00(±0.18)	5.81(±0.08)	5.73(±0.10)	7.74(±0.09)	7.61(±0.11)
ATLAS6	(6500, 4.0, 1.00)	1.5	4.78(±0.07)	4.93(±0.19)	5.53(±0.08)	5.78(±0.11)	7.48(±0.08)	7.66(±0.10)
		2.0	4.74(±0.07)	4.86(±0.16)	5.49(±0.09)	5.70(±0.10)	7.41(±0.11)	7.56(±0.12)
ATLAS6	(7000, 4.0, 1.00)	1.5	5.16(±0.10)	5.05(±0.21)	5.83(±0.10)	5.78(±0.11)	7.80(±0.10)	7.69(±0.10)
		2.0	5.11(±0.09)	4.98(±0.18)	5.78(±0.08)	5.71(±0.10)	7.72(±0.10)	7.60(±0.11)
ATLAS9	(6500, 4.0, 1.25)	1.5	4.91(±0.07)	5.01(±0.20)	5.65(±0.08)	5.86(±0.11)	7.60(±0.08)	7.73(±0.10)
		2.0	4.86(±0.07)	4.93(±0.16)	5.61(±0.09)	5.78(±0.10)	7.52(±0.11)	7.63(±0.11)
ATLAS9	(7000, 4.0, 1.25)	1.5	5.29(±0.10)	5.14(±0.22)	5.95(±0.10)	5.87(±0.11)	7.92(±0.09)	7.77(±0.10)
		2.0	5.24(±0.09)	5.07(±0.18)	5.91(±0.08)	5.79(±0.10)	7.84(±0.09)	7.68(±0.09)

Notes. The 1st and 2nd column describe the used model atmospheres, the adopted microturbulent velocity is in the 3rd column, and the resulting averaged abundances (±r.m.s. deviation) for each of the species are given in the 4th through 9th columns. The numbers of the lines used for averaging are indicated in the parentheses after each of the species names.

orbital elements of this binary system (cf. Steffen 1985).

Appendix 2. Microturbulence in the Atmosphere of Procyon

Motivated by the fact that the choice of the microturbulence plays a significant role in determining the Procyon's potassium abundance from the saturated K I 7699 line, we decided to investigate the nature of the microturbulent velocity field in the atmosphere of Procyon, by reanalyzing the equivalent-width data of Ti I/II, Cr I/II, and Fe I/II lines taken from table 4 of Kato and Sadakane (1982).

Our ξ-determination method is the same as that adopted by Takeda (1992; see subsection 2.1 therein), in which the depth-dependence of ξ in the atmosphere of Arcturus was studied by invoking the technique developed by de Jager et al. (1984). We exclusively used the gf values given in the compilations of Fuhr et al. (1988) and Martin et al. (1988), while following the same procedure as that described in subsection 2.2 of Takeda (1992) regarding the abundance determination (e.g., the choice of the damping parameters).

The results are depicted in figures 8 and 9, which correspond to figure 1 and figure 3 of Takeda (1992), respectively. Note that the definition of $\overline{\log \tau}$ in this paper (such as in Paper III or Takeda and Takada-Hidai 1994) is slightly different from that adopted in Takeda (1992); i.e., the use of $\tau_\lambda = 2/3$ instead of $\tau_\lambda = 1$ in equation (1) therein.

It can be clearly seen from figure 9 that ξ tends to decrease along with an increase in the atmospheric height from $\xi \sim 2.5$ km s^{-1} ($\tau_{5000} \sim 10^0$) to $\xi \sim 1.3$ km s^{-1} ($\tau_{5000} \sim 10^{-1}$); this tendency is just the opposite to the case of Arcturus (Takeda 1992). We suspect that the frequently quoted ξ value of 2 km s^{-1}, which has so far been derived by several authors and is regarded as being mostly established, simply reflects the averaged value of such a depth-dependent microturbulence.

We also point out, as a related evidence which may support the above finding, that application of our MPF method to the O I 7771–5 triplet lines of Procyon yields $\xi = 2.4$ km s^{-1} and $\log \epsilon_{\rm O}^{\rm NLTE} = 8.93$ (by following the similar procedure to that described in subsection 4.4 of Paper I). It may be reasonable to interpret this somewhat large ξ value as being due to the deep-forming nature of these high-excitation oxygen lines ($\chi = 9.15$ eV).

Appendix 3. On the Ionization Balance in the Atmosphere of Procyon

We here consider whether or not the LTE ionization balance is accomplished in the model atmospheres of Procyon discussed in appendix 1, based on the reanalysis of the equivalent widths of iron-group elements described in appendix 2.

We present in table 7 the averaged abundances of Ti, Cr, and Fe, which were derived from the same lines as those adopted for the ξ-determination (appendix 2), in order to see how the condition of ionization equilibrium is affected by changing the model parameters. The following points are concluded by closely inspecting this table.

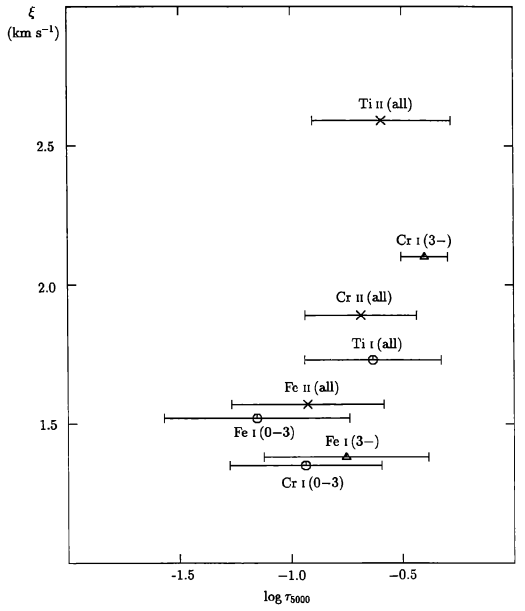

Fig. 9. Dependence of the microturbulent velocity upon the mean depth of line formation, derived for each group of the lines (cf. figure 8). The location of each symbol corresponds to the averaged mean-formation-depth over all lines belonging to the group, while the horizontal bar indicates the amount of the r.m.s. deviation.

— There still remains a small (but appreciable) discrepancy amounting to 0.1–0.2 dex between the LTE abundances from neutral and ionized species as far as the ATLAS6 model with $T_{\rm eff} \simeq 6500$–6600 K (which we consider as being the best Procyon model) is concerned, which is yet to be explained (e.g., by a non-LTE overionization effect).

— If we adopt the ATLAS9 model with $T_{\rm eff} \simeq 6700$–6800 K, which can reproduce the observed energy distribution, we can see that the LTE ionization equilibria turn out to be nearly accomplished for this case (reflecting the higher $T_{\rm eff}$). However, we tend to regard this coincidence as being merely fortuitous; this model had better be excluded for the reason mentioned in appendix 1.

— The resulting abundances are hardly affected by any choice of the mixing length (at least ATLAS6 models are concerned), which is naturally understood by recalling that even the continuum flux is insensitive to this parameter (cf. appendix 1). Hence, what was described in subsection 4.2 of Kato and Sadakane (1982) must be regarded as being incorrect, though the reason for such an erroneous result unfortunately can not be traced back.

References

Anders E., Grevesse N. 1989, Geochim. Cosmochim. Acta 53, 197

Andretta V., Gomez M.T., Severino G. 1991, Sol. Phys. 131, 1

Aymar M., Luc-Koenig E., Combet Farnoux F. 1976, J. Phys. B: Atom. Molec. Phys. 9, 1279

Blackwell D.E., Lynas-Gray A.E., Smith, G. 1995, A&A 296, 217

Bruls J.H.M.J., Rutten R.J. 1992, A&A 265, 257

Bruls J.H.M.J., Rutten R.J., Shchukina N.G. 1992, A&A 265, 237

Caccin B., Gomez M.T., Severino G. 1993, A&A 276, 219

de Jager C., Neven L. 1982, Ap&SS 84, 297

de Jager C., Mulder P.S., Kondo Y. 1984, A&A 141, 304

Fuhr J.R., Martin G.A., Wiese W.L. 1988, Atomic Transition Probabilities — Iron Through Nickel, J. Phys. Chem. Ref. Data Vol.17, Suppl. No.4 (American Chemical Society and American Institute of Physics for National Bureau of Standards)

Gerbaldi M., Faraggiana R., Castelli F. 1995, A&AS 111, 1

Gray D.F. 1981, ApJ 251, 152

Gray D.F. 1988, Lectures on Spectral-Line Analysis: F, G, and K Stars, (The Publisher, Arva, Ontario) ch1

Gray D.F. 1992, The Observation and Analysis of Stellar Photospheres, 2nd ed (Cambridge University Press, Cambridge) ch18

Griem H.R. 1974, Spectral Line Broadening by Plasmas (Academic Press, New York and London)

Hanbury Brown R., Davis J., Allen L.R. 1974, MNRAS 167, 121

Hirshfeld A., Sinnott R.W. 1985, Sky Catalogue 2000.0 Vol.2, Double Stars, Variable Stars and Non-stellar Objects, (Sky Publishing Corporation and Cambridge University Press, Cambridge)

Holweger H., Kock M., Bard A. 1995, A&A 296, 233

Holweger H., Müller E.A. 1974, Sol. Phys. 39, 19

Kato K., Sadakane K. 1982, A&A 113,135

Kato K., Watanabe Y., Sadakane K. 1995, PASJ submitted

Kiehling R. 1987, A&AS 69, 465

Kurucz R.L. 1979, ApJS 40, 1

Kurucz R.L., Furenlid I., Brault J., Testerman L. 1984, Solar Flux Atlas from 296 to 1300 nm, National Solar Observatory Atlas No.1 (Harvard University, Cambridge) (CD-ROM version)

Kurucz R.L., Peytremann E. 1975, Smithsonian Astrophys. Obs. Spec. Rept. No.362 (magnetic tape version)

Lambert D. 1993, Phys. Scripta T47, 186

Lambert D., Warner B. 1968, MNRAS 138, 181

Maltby P., Avrett E.H., Carlsson M., Kjeldseth-Moe O., Kurucz R.L., Loeser R. 1986, ApJ 306, 284

Martin G.A., Fuhr J.R., Wiese W.L. 1988, Atomic Transition Probabilities — Scandium Through Manganese, J. Phys. Chem. Ref. Data Vol.17, Suppl. No.3(American Chemical Society and American Institute of Physics for National Bureau of Standards)

Mathisen R. 1984, Oslo Inst. Theor. Astrophys. Publ. Series No.1

Moon T.T., Dworetsky M.M. 1985, MNRAS 217, 305

Moore C.E. 1971, Atomic Energy Levels Vol.I, NSRDS-NBS35 (US Government Printing Office, Washington DC)
Smith M.A. 1973, ApJ 182, 159
Steffen M. 1985, A&AS 59, 403
Takeda Y. 1992, A&A 253, 487
Takeda Y. 1994a, PASJ 46, 53
Takeda Y. 1994b, PASJ 46, 181
Takeda Y. 1995a, PASJ 47, 287 (Paper I)
Takeda Y. 1995b, PASJ 47, 337 (Paper III)
Takeda Y. 1995c, PASJ 47, 463 (Paper IV)
Takeda Y., Sadakane K., Takada-Hidai M. 1995, PASJ 47, 307 (Paper II)
Takeda Y., Takada-Hidai M. 1994, PASJ 46, 395
Travis L.D., Matsushima S. 1968, ApJ 154, 689
Unsöld A. 1955, Physik der Sternatmosphären, 2nd ed. (Springer, Berlin) p333
Wiese W.L., Smith M.W., Miles B.M. 1969, Atomic Transition Probabilities Vol.II – Sodium Through Calcium, NSRDS-NBS22 (US Government Printing Office, Washington DC)
Wynne-Jones I., Ring J., Wayte R.C. 1978, in High Resolution Spectrometry, Proc. 4th Colloquium Ap., ed M. Hack (Trieste Observatory) p519